iScience

CellPress
OPEN ACCESS

Article

# A mitochondria-targeting dihydroartemisinin derivative as a reactive oxygen species -based immunogenic cell death inducer

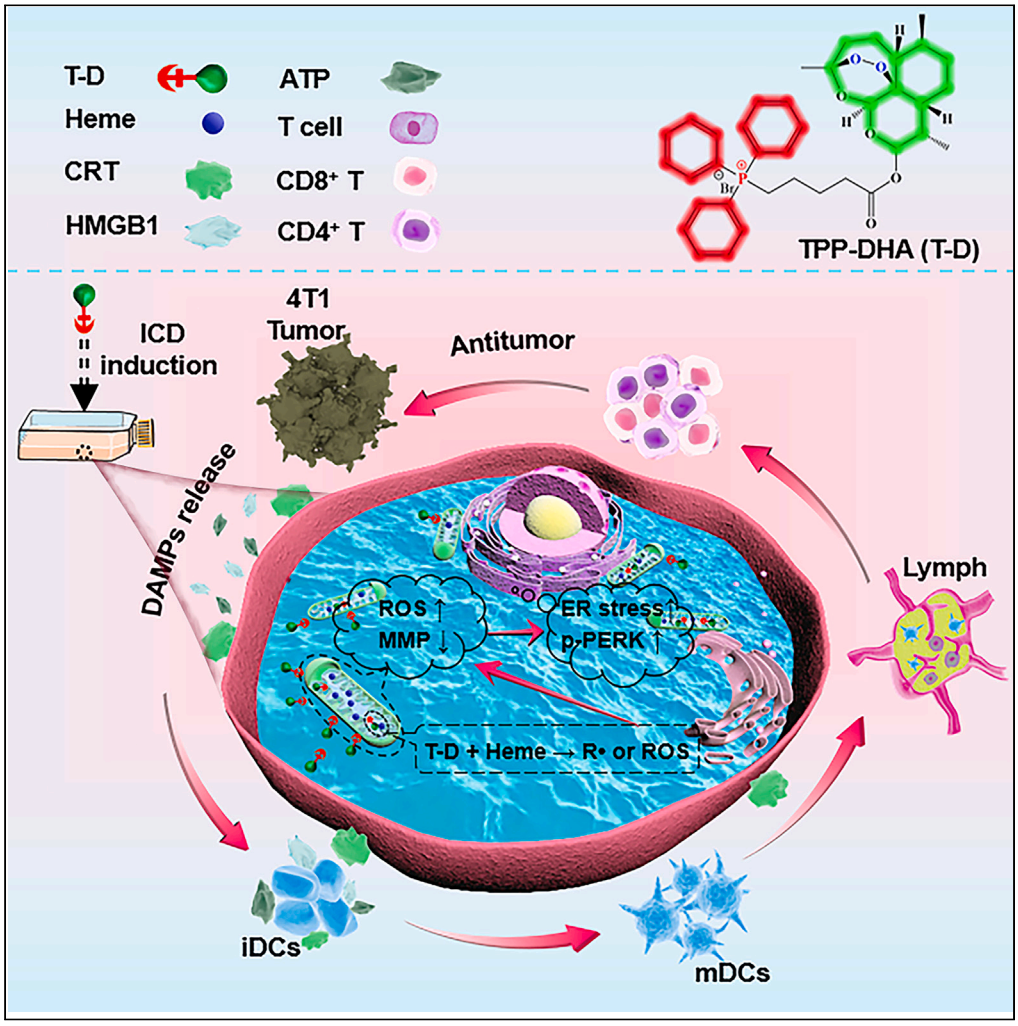


Hong-Yang Zhao, Kun-Heng Li, Dan-Dan Wang, Zhi-Li Zhang, Zi-Jian Xu, Ming-Hui Qi, Shi-Wen Huang

swhuang@whu.edu.cn

## Highlights

A mitochondria-targeting dihydroartemisinin derivative (TPP-DHA，T-D) was synthesized

T-D can selectively accumulate in mitochondria to trigger ROS generation

T-D exhibits far more potent ICD-inducing properties than its parent compound

Zhao et al., iScience *27*, 108702
January 19, 2024 
https://doi.org/10.1016/j.isci.2023.108702

iScience

CellPress
OPEN ACCESS

Article

# A mitochondria-targeting dihydroartemisinin derivative as a reactive oxygen species -based immunogenic cell death inducer

Hong-Yang Zhao,[1] Kun-Heng Li,[1] Dan-Dan Wang,[1] Zhi-Li Zhang,[1] Zi-Jian Xu,[1] Ming-Hui Qi,[1] and Shi-Wen Huang[1,2,*]

## SUMMARY

**Immunogenic cell death (ICD) can activate the anticancer immune response and its occurrence requires high reliance on oxidative stress. Inducing mitochondrial reactive oxygen species (ROS) is a desirable capability for ICD inducers. However, in the category of ICD-associated drugs, numerous reported ICD inducers are a series of anthracyclines and weak in ICD induction. Herein, a mitochondria-targeting dihydroartemisinin derivative (T-D) was synthesized by conjugating triphenylphosphonium (TPP) to dihydroartemisinin (DHA). T-D can selectively accumulate in mitochondria to trigger ROS generation, leading to the loss of mitochondrial membrane potential ($\Delta\Psi_m$) and ER stress. Notably, T-D exhibits far more potent ICD-inducing properties than its parent compound. *In vivo*, T-D-treated breast cancer cell vaccine inhibits metastasis to the lungs and tumor growth. These results indicate that T-D is an excellent ROS-based ICD inducer with the specific function of trigging vigorous ROS in mitochondria and sets an example for incorporating artemisinin-based drugs into the ICD field.**

## INTRODUCTION

The low immunogenicity of tumors is one of the main obstacles to the application of cancer immunotherapy.[1,2] Therefore, it is imperative to improve the immunogenicity of tumors for activating an immune response. In recent years, inducing the immunogenic cell death (ICD) of cancer cells serves as a promising approach to developing tumor immunogenicity.[3] ICD is a form of regulated cell death that occurs in stressed, injured, or dying cells and featured the emission of damage-associated molecular patterns (DAMPs) that can efficaciously trigger an anticancer immune response.[4] Three typical "danger" signals of DAMPs are identified as the hallmarks of ICD, including calreticulin (CRT), high-mobility group box 1 (HMGB1), and adenosine triphosphate (ATP).[5] In specific, CRT is exposed as "eat-me" signals on the cell surface to facilitate the phagocytosis of dendritic cells (DCs). Adenosine triphosphate (ATP) is released into the extracellular environment, acting as a "find me" signal for recruiting DCs to sites of active ICD. Furthermore, HMGB1 is liberated from the nucleus to the extracellular environment with the function of enhancing the antigen presentation effect of DCs. Their interactions with the immune system synthetically lead to converting a "cold" tumor microenvironment into a "hot," immunogenic one.[6,7] Since the mechanism of ICD induction is correlated to the ICD inducer itself, inducers can be classified into two types depending on whether they are selectively targeted to the endoplasmic reticulum (ER) or not.[8] Type I ICD inducers (e.g., doxorubicin, mitoxantrone, and paclitaxel) induce the emission of DMAPs through the non-ER-associated targets or reactive oxygen species (ROS).[9,10] Conversely, Type II ICD inducers can specially target the ER to disturb ER homeostasis, thereby causing ER stress and ICD.[11–13] The process of ICD induction is highly stressor-dependent, growing strategies have been executed for designing small-molecule agents, metallic compounds, or nano-platforms as inducers to induce ICD by evoking stress in cancer cells.[14–17]

Mitochondria are vital for the maintenance of cellular physiological function due to their role as cellular powerhouses, metabolic and signal transduction centers.[18] Studies have reported that mitochondria and ER jointly maintain cellular homeostasis by exchanging metabolites and ions across the mitochondria-associated ER membrane (MAMs).[19,20] So, the physiological state of each organelle is affected by the other.[21] For instance, calcium ions overload in mitochondria can increase ROS further leading to ER stress.[22–24] Thus, it may be a potential way here that the induction of ICD is achieved by triggering ROS generation in mitochondria. Indeed, mitochondria-targeting agents or nano-materials have been reported to significantly enhance ICD effects by inducing mitochondrial ROS in a spatiotemporal control manner (e.g., photodynamic and sonodynamic modalities).[25,26] Moreover, our pervious study proved that equal amounts of ROS generated in the mitochondria can induce stronger ICD effects than generation in the cytoplasm.[27] In this respect, endowing agents with mitochondrial targeting is necessary for inducing a large-scale ICD.

[1]Key Laboratory of Biomedical Polymers of Ministry of Education, Department of Chemistry, Wuhan University, Wuhan 430072, People's Republic of China
[2]Lead contact
*Correspondence: swhuang@whu.edu.cn
https://doi.org/10.1016/j.isci.2023.108702

Dihydroartemisinin (DHA), a derivative of artemisinin containing the peroxy group, has been confirmed and recommended by the World Health Organization (WHO) as a safe and effective antimalarial drug.[28] The peroxy group that endows its antimalarial and anticancer activity can react with ferrous ions or heme to form highly reactive and toxic carbon-centered free radicals, leading to the alkylation of target proteins and oxidative stress in cells.[29–32] Currently, there are few studies on the role of DHA in inducing ICD, and the non-specific distribution of DHA in the cytoplasm results in a mild ICD effect.[33] We posited that the potential of ICD induction has not been fully realized due to the lack of mitochondria-targeting of DHA itself. As we all know, heme is produced in the mitochondria and acts as an activator of dihydroartemisinin. Capitalizing on this, we tried to deliver DHA into the mitochondria for reaction with heme to induce ICD by mitochondrial ROS production, known as the pattern of Type I ICD induction. Encouraged by previous works, triphenylphosphonium (TPP), a lipophilic cationic unit, was used as a mitochondrial-targeting ligand for effective delivery of drugs to selectively localize in the mitochondria with a highly negatively charged membrane potential ($\Delta\Psi$m, −220 mV).[34] Based on this fact, a mitochondria-targeting dihydroartemisinin derivative TPP-DHA (named T-D) was synthesized by linking triphenylphosphonium (TPP) to dihydroartemisinin (DHA). In this work, we proved that T-D efficaciously heightens ICD-associated DAMPs release more than non-mitochondrial-targeting DHA because of its specific mitochondria-targeting and higher ROS generation capability in mitochondria. Additionally, considering that the effect of the cancer cell vaccine-induced immune response is mainly dependent on the expression quantity of its surface CRT, we optimized the dose and treatment time of T-D-treated cancer cells to identify the optimal conditions for the highest CRT expression. Inspiringly, the prophylactic tumor vaccination experiment demonstrated that the T-D-treated cell vaccine can effectively excite the body to establish a robust immune response, form a long-lasting immune memory, and strengthen the immunotherapy efficacy against cancer. In brief, T-D is a ICD inducer, which expands the application of artemisinin analogs in ICD research.

## RESULTS

### Characterization of triphenylphosphonium- dihydroartemisinin

TPP-DHA (T-D) was synthesized from dihydroartemisinin (DHA) and TPPBr-$(CH_2)_4$-COOH by a one-step esterification reaction, which is shown in Figure S1.[34] The intermediate TPPBr-$(CH_2)_4$-COOH and target product TPP-DHA were characterized with $^1$HNMR spectra (Figures S2 and S3). The structure of T-D were confirmed by $^{13}$C NMR and ESIMS (Figures S4 and S5).

### Cell viability test *in vitro*

MTT assay results in Figure 1A demonstrated that the cytotoxicity of T-D against 4T1 cells with an $IC_{50}$ value of 1.3 μM was stronger than DHA with an $IC_{50}$ value of 4.5 μM. In addition, cytotoxicity and $IC_{50}$ of T-D against CT26, HeLa, and MCF-7 cell lines were shown in Figure S6. In comparison of DHA, TPP-modified DHA is able to easily accumulate in the mitochondria of cancer cells and react with abundant mitochondrial heme in cancer cells to generate large amount of toxic ROS. Simultaneously, the effects of DHA and T-D on the viability of 4T1 cells were evaluated using live-dead cell staining. As shown in Figure 1B, in the case of DHA-treated 4T1 cells, there was strong green fluorescence from live cells stained with Calcein-AM and weak red fluorescence from dead cells stained with Pyridine Iodide, indicating the low ability of DHA to kill 4T1 cells. In contrast, negligible green fluorescence and strong red fluorescence was observed in T-D-treated 4T1 cells. These results are consistent with MTT assay results. The quantitative analysis of apoptosis with flow cytometry, shown in Figure 1C, demonstrated that the total apoptosis rate of 4T1 cells induced by T-D was 35.8%, which was remarkably higher than that of DHA at 7.76%. Taken together, T-D showed remarkable enhancement in cytotoxicity compared with DHA which was attributed to the enrichment of DHA in mitochondria by the incorporation of cationic TPP unit.

### Analysis of reactive oxygen species generation

ROS are essential for regulating various physiological functions of living organisms, while excessive ROS production causes the disruption of intracellular redox homeostasis, the depolarization of the mitochondrial membrane, up-regulation caspase level, and induction apoptosis.[35] DCFH-DA and Mito-tracker Red were used as fluorescent probes to monitor the generation and intracellular location of ROS in 4T1 cells after separate treatment with DHA and T-D at a concentration of 2.5 μM for different time (6 h, 12 h, 18 h, 24 h). The confocal laser scanning microscopy (CLSM) images, shown in Figure 1D, demonstrated that both DHA and T-D treatments induced the generation of ROS in 4T1 cells. The intensities of green fluorescence of DCF, generated from DCFH and ROS in the cells, increased with the increase of incubation time together with DHA or T-D, suggesting that the level of intracellular ROS production gradually increased, however, after the same treatment time, T-D induced generation of more ROS than DHA. In addition, in the case of DHA-treated cells, non-overlap of green fluorescence and red fluorescence from Mito-tracker Red for labeling the mitochondria indicated that generated ROS did not locate in the mitochondria. Differently, ROS in 4T1 cells treated with T-D for 12 h mainly located the mitochondria since the green and red fluorescence well overlapped in the cells. Further incubation of 4T1 cells with T-D (18 or 24 h) resulted in serious mitochondrial damage. The seriously damaged mitochondria could not be labeled with Mito-tracker Red. Furthermore, the level of ROS production was quantified by flow cytometry analysis, as shown in Figures S7, 1E, and 1F). It was found that the ROS production in different groups was time-dependent. For example, after treatment with T-D for 6 h, 12 h, 18 h, and 24 h, the percentages of $ROS^+$ cells increased from 9.6% to 10.4%, 17%, and 21%, respectively. At all incubation time point, T-D-treated cell showed more ROS generation ability than DHA-treated cells. Similar results were obtained in the mean fluorescence intensity values (MFI) of cells separately treated with DHA and T-D, which are also consistent with fluorescent imaging results with CLSM.

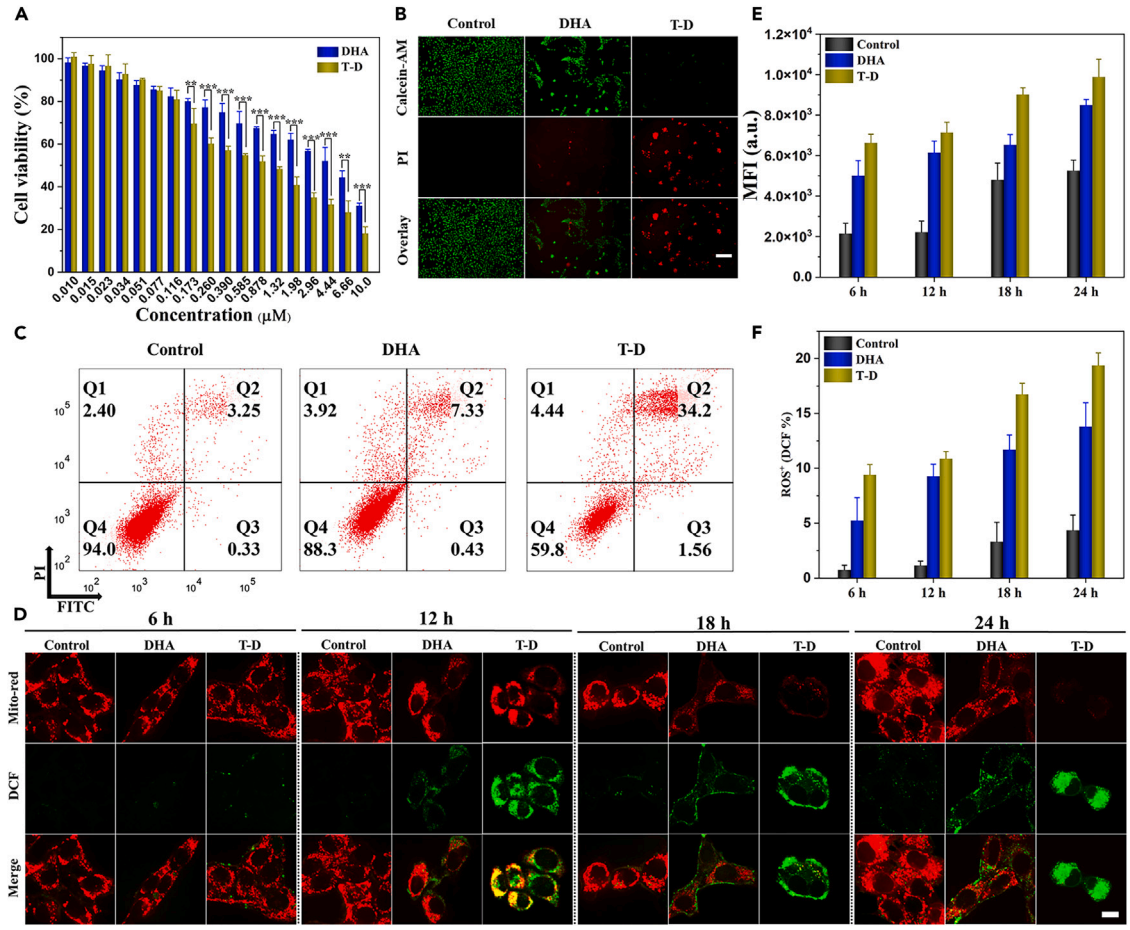


**Figure 1. Cell viability and ROS detection**

(A) *In vitro* cell viability of 4T1 cells after being treated with DHA and T-D. Data are presented as mean ± S.D. (n = 3), *p < 0.05, **p < 0.01, ***p < 0.001, by one-way analysis of variance (ANOVA).

(B) 4T1 cells after being treated with DHA and T-D, which were stained with Calcein-AM/PI to observe the living or dead cells, scale bar = 200 μm.

(C) Cell apoptosis assay of 4T1 cells after incubation with DHA or T-D for 24 h.

(D) CLSM images of 4T1 cells for ROS generation (green fluorescence) after treatment with DHA or T-D at different times, scale bar = 10 μm.

(E) The MFI value of DCF was measured by flow cytometry.

(F) Percentages of $ROS^+$ expression in 4T1 cells.

## Evaluation of mitochondrial depolarization

Mitochondrial membrane potential ($\Delta\Psi m$) is closely related to the physiological state of cells. The effects of T-D and DHA on $\Delta\Psi m$ were evaluated using JC-1 dye. JC-1 fluoresces red as aggregate in the mitochondrial matrix with high $\Delta\Psi m$, while fluoresces green as a monomer in the damaged mitochondrial matrix with low $\Delta\Psi m$. As shown in Figure S8, stronger green fluorescence was observed in cells treated with T-D for 12 h, certifying that mitochondrial damage manifested as a decrease in $\Delta\Psi m$, while the green fluorescence was weak in the DHA group. After 24 h, the red fluorescence of the T-D group almost disappeared and showed strong green fluorescence compared with the DHA group, demonstrating that the mitochondria were severely disrupted and attenuated $\Delta\Psi m$ significantly. In addition, a quantitative analysis of $\Delta\Psi m$ changes was shown in Figures 2A and S9. The proportion of green fluorescence increased from 14.4% (46.7%) to 34.4% (88.6%) after cells were treated with DHA (T-D) from 12 h to 24 h, respectively, which means that the relative Red/Green ratio in the T-D group was significantly lower than the DHA group, providing solid evidence for T-D enhanced $\Delta\Psi m$ decrease via mitochondrial targeting (Figure 2B).

## Detection of immunogenic cell death effect

After stimulation by certain agents, cells release some immunogenic cellular contents such as CRT, HMGB1 and ATP, a process known as immunogenic cell death (ICD).[36,37] Firstly, to investigate whether T-D could massively evoke ICD, the CRT exposure on the surface of cells was quantified analysis (Figure S10). We speculated that the expression of CRT could be related to the agent, dose, and duration of treatment. Then CRT was measured after cells incubation with T-D at different concentrations (0.5 μM, 1 μM, 2 μM, 2.5 μM, 3 μM) and different times (12 h,

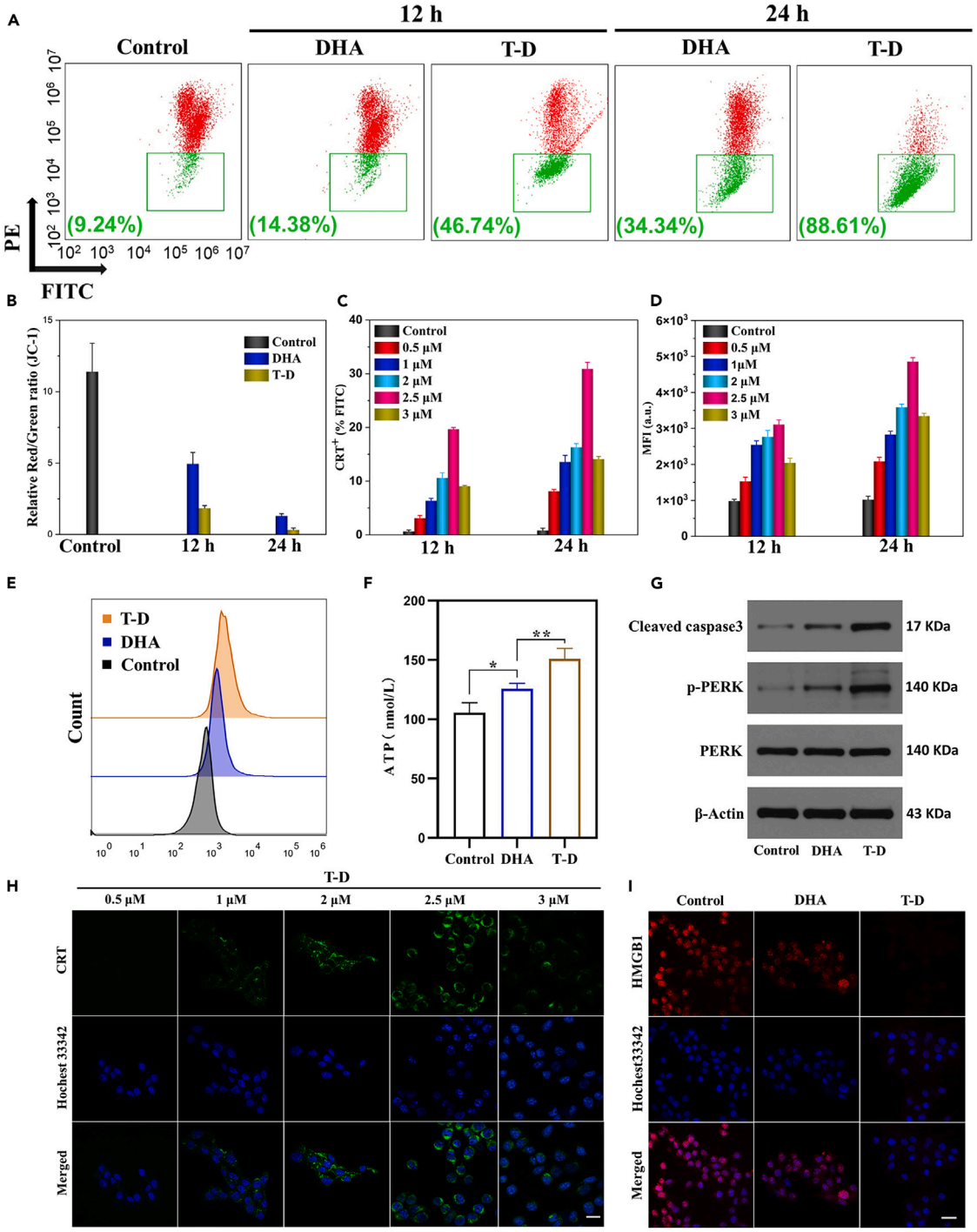


**Figure 2. Mitochondrial damage and ICD detection**

(A) 4T1 cells treated with different formulations and stained with JC-1 were analyzed with flow cytometry.

(B) Statistical analyses of the relative ratio of JC-1 aggregate (red)/JC-1 monomer (green).

(C) Percentages of $CRT^{+}$ expression in 4T1 cells.

(D) The MFI value of CRT was measured by flow cytometry.

(E) Flow cytometry analyses of the exposed CRT on the surface of 4T1 cells incubation with DHA and T-D, respectively.

**Figure 2. *Continued***

(F) Quantitative analyses of ATP in the cell supernatants after 4T1 cells were treated with DHA and T-D, respectively. Data are presented as mean ± S.D. (n = 3), ***p < 0.001, **p < 0.01, and *p < 0.05.

(G) Western blotting analysis of apoptosis-related proteins in 4T1 cells treated by PBS, DHA, and T-D.

(H) CRT translocation onto the cellular membrane was observed by CLSM after the 4T1 cells incubation with T-D, scale bar = 10 μm.

(I) CLSM images showing HMGB1 release from the nucleus of 4T1 cells treated with DHA or T-D, respectively, scale bar = 10 μm.

24 h). As shown in Figures 2C and 2D, after the cells were co-incubated with T-D for 12 h, it was found that $CRT^+$ expression was highest and the MFI value reached the maximum at a concentration of 2.5 μM. Notably, after 24 h, the results were still in accordance with the above, but $CRT^+$ expression was 1.56 times higher than before. Therefore, this optimal drug concentration guided the subsequent experiments and proved that the previous hypothesis was valid. Additionally, as shown in Figure 2H, it was observed by CLSM that the intensity of green fluorescence of CRT changed with the increase of T-D drug concentration from 0.5 μM, 1 μM, 2 μM, 2.5 μM, and 3 μM. As expected, the green fluorescence was strongest at a concentration of 2.5 μM, which is consistent with the above outcome obtained by flow cytometry analysis. In contrast to the T-D group, the green fluorescence was weak with no significant regular changes in the DHA group (Figure S11). Simultaneously, cells were treated with both T-D and DHA at concentrations of 2.5 μM for 24 h, respectively, the fluorescence intensity of CRT in the T-D group was greater than the DHA group (Figure 2E). In conclusion, under the same experimental condition, there was a significant difference in CRT expression after cells were treated with T-D and DHA, respectively. It is this difference that proved the important role of DHA in targeting mitochondria to generate excess ROS and thus induce CRT expression. HMGB1 is a typical representative of endogenous alarmin. Under normal physiological conditions, it belongs to intracellular DNA-binding protein with functions of stabilizing nucleosomes and regulating gene transcription, but when cells are necrotic by external factors, it will be released from the nucleus to the extracellular environment.[38] To explore whether T-D can induce HMGB1 release, as shown in Figure 2I, the significantly reduced red fluorescence was observed in the nucleus and cytoplasm, indicating that a considerable amount of HMGB1 was released from the nucleus to the extracellular environment. However, showy red fluorescence could still be observed in the nucleus and cytoplasm for the DHA group, and mainly localized to the nucleus in the Control group. The level of ATP secretion was detected to further confirm the ability of T-D to induce ICD. It was shown that the amount of extracellular ATP secreted in the supernatant from the T-D group was 1.2 times higher than the DHA group (Figure 2F). ICD-inducing properties of T-D in other cell lines were also performed (Figures S12—S14). Additionally, T-D demonstrated stronger ICD-inducing ability compared to DOX, a traditional ICD inducer (Figure S15). These results comprehensively indicated that T-D is an excellent ROS-based ICD inducer owing to its focused mitochondrial-targeting and efficient ROS production ability.

## Analysis of apoptosis-related proteins

Excessive production of ROS alters the outer mitochondrial membrane permeability, causing mitochondria to release apoptosis-related factors into the cytoplasm, ultimately triggering caspases-dependent apoptosis via an endogenous pathway initiated from the mitochondria.[39] Cleaved-caspase-3 is the activated form of caspase-3 produced by the cascade effect of caspases, and its presence indicates the cell enters the execution phase of the apoptotic effect.[40] As shown in Figure 2G, Cleaved-caspase-3 was upregulated in the T-D group in contrast to the DHA group, indicating that T-D induced apoptosis more efficaciously through the mitochondrial pathway than DHA. The endoplasmic reticulum (ER) also plays a pivotal role in maintaining cellular $Ca^{2+}$ homeostasis as well as protein and lipid production, processing, and transport.[41] When ROS enter the ER to generate oxidative stress, it causes the dissociated PERK to undergo autophosphorylation to form p-PERK.[42] More importantly, a much higher protein level of p-PERK was observed in the T-D group compared with the DHA group. Collectively, these results suggested that mitochondrial ROS could evoke ER stress which is most likely related to crosstalk between ER and mitochondrial ROS through MAMs.[43]

## Dendritic cell maturation and cytokine detection *in vitro*

Dendritic cells (DCs) are the protagonist for the uptake, processing and presentation of antigens, and its process of maturation induced by ICD is always accompanied by the secretion of cytokines such as interleukin-6 (IL-6) and tumor necrosis factor (TNF-α).[44] As shown in Figures 3A and 3B, the proportion of mature DCs was 53.8% in the T-D group, which was obviously higher than those groups of DHA 46.1%, X-ray 40.8%, and Control 36.1%. So, the T-D-treated cell vaccine exhibited the best effect for eliciting the activation of DCs. Additionally, IL-6 and TNF-α as indicators of DC activation were detected by ELISA. These results showed that the secretion levels of IL-6 and TNF-α from DCs suspensions in the T-D group were well above those in others, demonstrating that T-D-treated cell vaccine could evoke strong antitumor immunity thanks to the induction of the "eat me" signal by ICD (Figures 3C and 3D).

## Immune response *in vivo*

Initially, one week after twice vaccination, the mice in each group were sacrificed and the inguinal lymph nodes were isolated for evaluating DCs maturation during the adaptive immune response by flow cytometry. As displayed in Figures 4A and 4B), the proportion of mature DCs ($CD80^+CD86^+$) in the T-D group (≈28.6%) was dramatically higher than those in the other three groups (≈18%, ≈15%, and ≈10.2% for DHA, X-ray, and Control group, respectively). The result firmly proved that the T-D-treated cell vaccine gave the best performance in the uptake of antigens by DCs and the promotion DCs maturation.

Initial T cells are stimulated by antigens and proliferate and differentiate into helper T cells ($CD3^+CD4^+$) and cytotoxic T cells ($CD3^+CD8^+$) under different conditions, where $CD3^+CD4^+$ T cells with assisting the function of humoral and cellular immunity and $CD3^+CD8^+$ T cells can

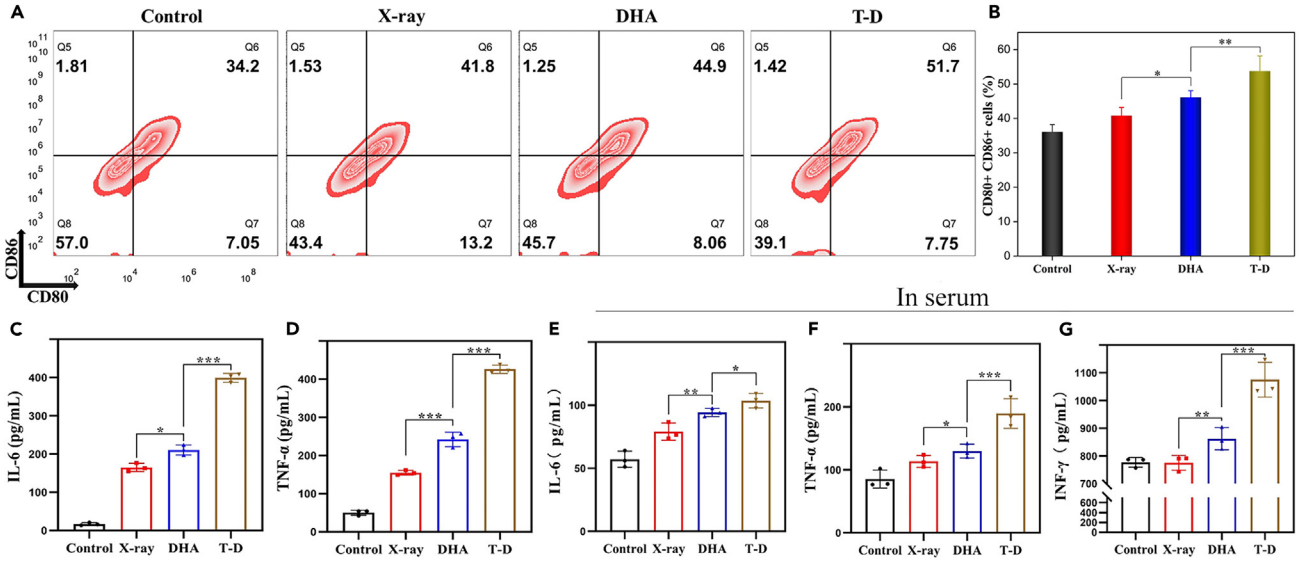


**Figure 3. Analysis of mature DCs and cytokine level**

(A) Representative analytical results of mature DCs by the markers ($CD80^+$ $CD86^+$).

(B) Histogram analysis of mature DCs after the immature DCs were cultured with different treated 4T1 cell vaccines.

(C) IL-6 and (D) TNF-α in DCs suspensions.

(E) IL-6, (F) TNF-α, and (G) INF-γ levels in the serum of the mice. Data are presented as mean ± S.D. (n = 3), ***p < 0.001, **p < 0.01, and *p < 0.05.

specifically kill target cells.[45,46] To intrinsically verify whether the T-D-treated cell vaccine can induce the formation of a systemic immune response, a series of immune cells in the spleen were analyzed by flow cytometry using T-distribution distributed stochastic neighbor embedding (t-SNE, Figure 4C), and the corresponding results are shown in Figure 4D. No significant changes in $CD3^+CD8^+$ T cell proliferation in spleens of mice severally treated with PBS, DHA-treated cell vaccine, and X-ray-treated cell vaccine (21.2%, 21.6%, and 21.8%). Observably, the T-D-treated cell vaccine appreciably improved the proportions of $CD3^+CD8^+$ T cells (23%). Moreover, the percentage of $CD3^+CD4^+$ T cells in total T cells ($CD3^+$) was 16.8%, 19.8%, 28.2%, and 34.1% in the Control, X-ray, DHA, and T-D groups, respectively. Similarly, it was found that Th1($CD4^+IFN\text{-}\gamma^+$) cells also increased sequentially in the order of the above groups, 1.89%, 3.64%, 5.04%, and 6.03%, and it secretes the cytokine IFN-γ that activates macrophages and promotes cytotoxic T cells ($CD8^+IFN\text{-}\gamma^+$) maturation. Meanwhile, immune memory T cell was evaluated to determine whether the T-D-treated cell vaccine could effectively induce an immune memory effect. Memory T cells ($T_M$) include $CD4^+$ $T_M$ and $CD8^+$ $T_M$, each of which is subdivided into effective memory T cell ($T_{EM}$), central memory T cell ($T_{CM}$), and so on, where $T_{EM}$ has a rapid-onset effector function, while $T_{CM}$ is incapable of directly exerting an effector function and need to differentiate into $T_{EM}$ again upon antigen stimulation to participate in the memory response.[47] As shown in Figure 4D, the proportions of CD4 $T_{EM}$ ($CD4^+$ $CD44^+CD62L^-$), CD4 $T_{CM}$ ($CD4^+CD44^+CD62L^+$), CD8 $T_{EM}$ ($CD8^+CD44^+CD62L^-$) and CD8 $T_{CM}$ ($CD8^+CD44^+CD62L^+$) all showed an increasing trend in the order of Control, X-ray, DHA, and T-D groups, as well as cytotoxic T cells ($CD8^+IFN\text{-}\gamma^+$), suggesting that the T-D-treated cell vaccine can effectively increase frequency of memory T cells and successfully trigger anti-tumor immune memory in mice. Cytokine secretion is equally vital during the innate and adaptive immune response. Cytokines have physiological properties such as pleiotropism, redundancy, synergy, and antagonism, and when combined with the corresponding receptors, they participate in regulating many important physiological functions such as cell growth, differentiation, and immune response, further form a complex cytokine regulatory network.[48] CRT can stimulate DCs to secrete pro-inflammatory IL-6 and TNF-α, among that IL-6 can promote B lymphocytes proliferation and differentiation, and synergistically stimulate T cell proliferation and activation with TFN-α and IFN-γ secreted by activated $CD4^+$ cells and $CD8^+$ T cells potentiate anti-tumor effects.[49] So, the level of IL-6, TNF-α, and IFN-γ in peripheral blood serum was analyzed by ELISA (Figures 3E–3G). Compared with other groups, the T-D group showed the highest levels of IL-6, TNF-α, and IFN-γ (IL-6: 1.1-, 1.4- and 1.8-fold greater than DHA, X-ray, and Control groups, respectively; TNF-α: 1.5-, 1.8- and 2.2-fold greater than DHA, X-ray and Control groups, respectively; IFN-γ: 1.2-, 1.4- and 1.4-fold greater than DHA, X-ray and Control groups, respectively). These significant differences indicated that the antigen-presenting ability of DCs could be effectively stimulated by the T-D-treated cell vaccine, making DCs secrete high levels of pro-inflammatory cytokines IL-6 and TFN-α synergistically activated T cells to secrete IFN-γ, which further mediated cellular immune responses and eventually formed an anti-tumor immune environment. Finally, a lung metastasis model was executed to explore the long-term immunological memory effects of an ICD-induced cancer vaccine. As shown in Figures 4E, S16, and S17, mice vaccinated with T-D-treated cells had fewer tumor metastases in the lungs, and the size and number of lung metastasis tumors were remarkably reduced relative to the other three groups which agreed well with the results in H&E staining analysis. Altogether, these data demonstrated that the ICD effect evoked by mitochondrial ROS could augment the maturation of DCs, the proliferation of $CD4^+$ or $CD8^+$ T cells, and the secretion of cytotoxic cytokines, furthering the overall establishment of a robust anti-metastatic immune system.

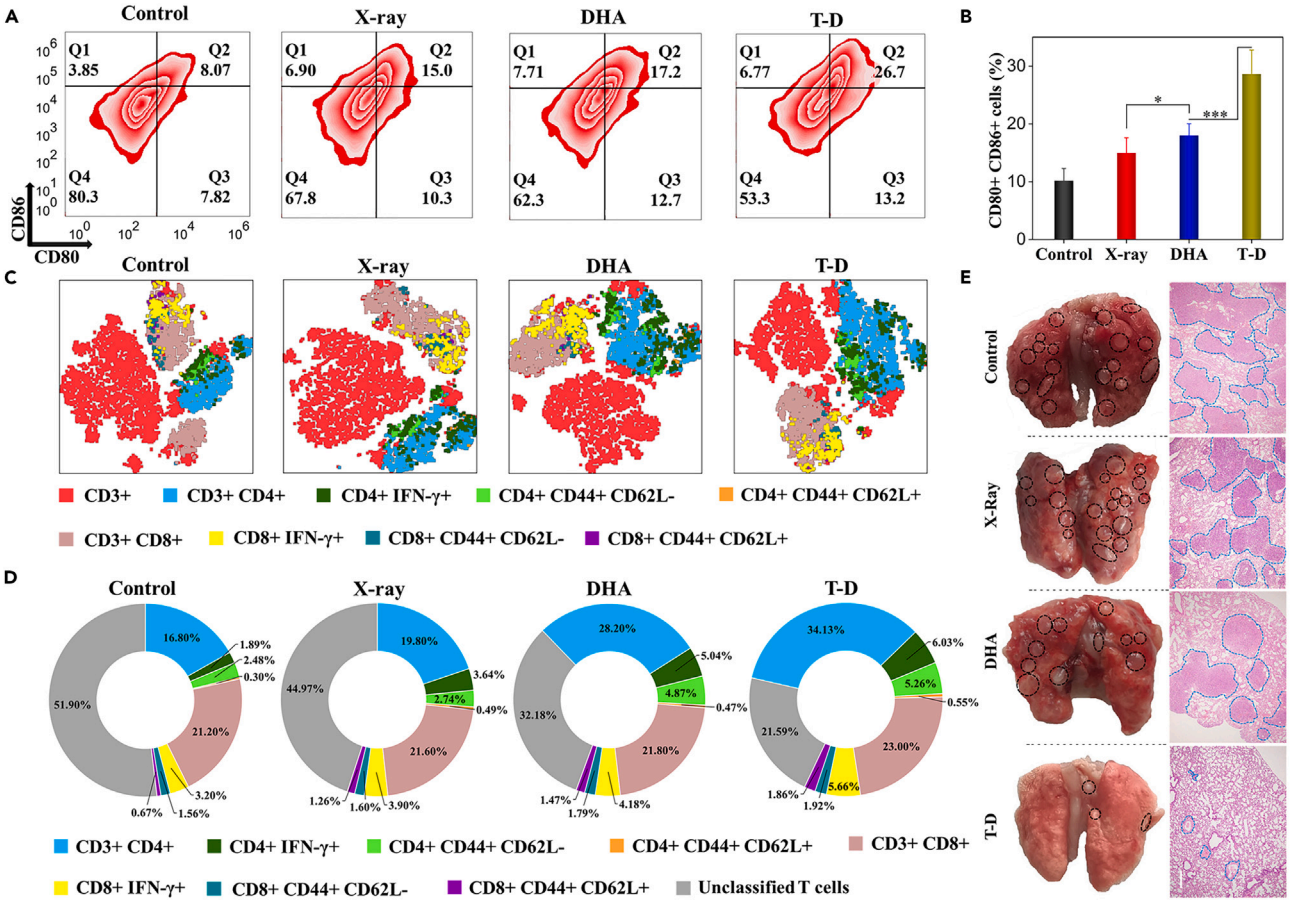


**Figure 4. Analysis of immune cells, cytokine level and anti-metastatic *in vivo***

(A) Inguinal lymph nodes were harvested to measure the percentage of mature DCs by the markers ($CD80^+CD86^+$).

(B) histogram analysis of mature DCs. Data are presented as mean ± S.D. (n = 3), ***p < 0.001, **p < 0.01, and *p < 0.05.

(C) T-distributed stochastic neighbor embedding (t-SNE) visualization.

(D) Quantification of different immune T cells in spleen by flow cytometry.

(E) Images of lung tissue from mice in different groups, black dashed lines indicate the sites of lung metastatic nodules. HE staining of lungs, the blue circles indicate metastatic foci, scale bar = 200 μm.

## Tumor prevention effect

To further conclude whether T-D is an ICD inducer, it was determined by the golden standard of vaccination experiments.[50] As displayed in tumor growth curves in Figure 5A, after the inoculation of live 4T1 cells, the tumors of mice in Control, X-ray, and DHA groups showed rapid growth compared with those in the T-D group, the mean tumor volume in the T-D group was 519 $mm^3$ at day 34, 2.5-, 3.5- and 3.8-fold smaller than DHA, X-ray, and Control groups, respectively (Figure 5B). T-D-treated cell vaccine exhibited superior antitumor ability with a growth suppression rate of 72.4%. Undoubtedly, the vaccines of DHA-treated cells and X-ray-treated cells failed to suppress the tumor growth as effectively as that of T-D-treated cells, as proved by the final average tumor weight of ≈0.62 g, ≈0.56 g, and ≈0.23 g for X-ray, DHA, and T-D groups, respectively (Figure 5C). Meanwhile, as shown in Figure 5I, the H&E assay showed the highest cancer necrocytosis and lowest proliferation ability in the T-D groups. Encouragingly, the first mouse death occurred in the T-D group on day 51, while the other three groups all died before day 44 after rechallenging with live 4T1 cell (Figure 5H). These data revealed that the T-D-treated cell vaccine exhibited good inhibition of tumor growth, which attributed to the fact that the expression of CRT in cells induced by T-D could effectively elicit an anti-tumor immune memory effect.

Reviewing the results of the aforementioned experiments, during treatment with mitochondria-targeting T-D, 4T1 cells were induced with powerful ICD effects and formulated into vaccines that could stimulate adaptive immune responses such as the maturation of DCs and proliferation of $CD4^+$ or $CD8^+$ T cells. Presently, to verify the underlying mechanisms of antitumor immunity described above, a series of immune cells in lymph nodes and tumor tissues were analyzed. Results in Figures 1B and 5D–5G showed that the increased number of mature DCs, CD8 $T_{EM}$ ($CD8^+CD44^+CD62L^-$), and cytotoxic T cells ($CD8^+IFN\text{-}\gamma^+$), but decreased number of $T_R$ cells ($CD4^+CD25^+Foxp3^+$) T cells in the group of T-D. Furthermore, the levels of caspase-3 in tumor cells and $CD8^+$ T cell infiltration in tumors were further evaluated with

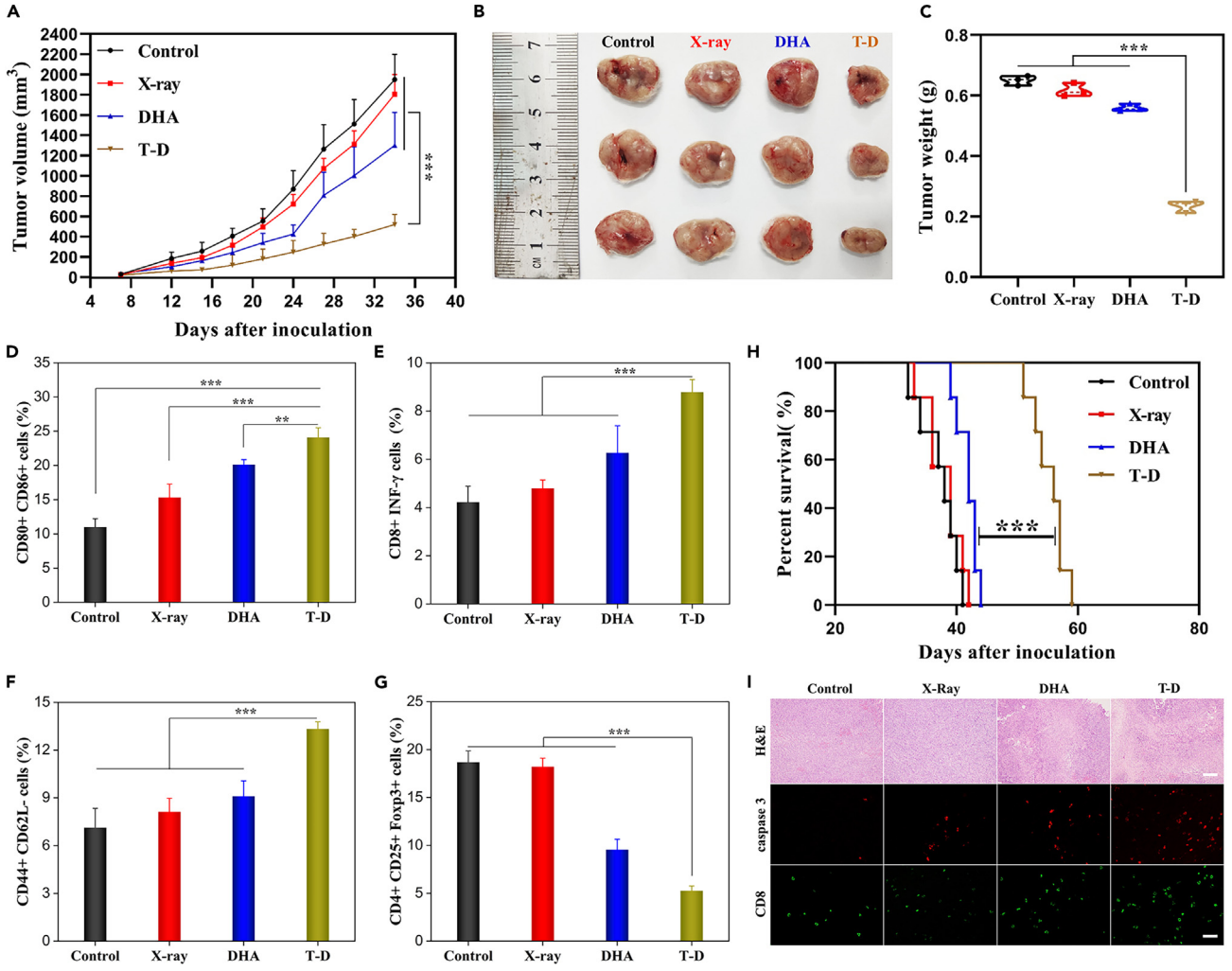


**Figure 5. Evaluation of antitumor effect *in vivo***

(A) Changes of averaged tumor volume after challenge, (n = 10).

(B) Digital photographs and (C) weight of tumors separated from mice after different treatments, (n = 3).

(D) Flow cytometric analyses of the populations of mature DCs ($CD80^+$ $CD86^+$) in inguinal lymph nodes of mice immunized by various vaccine formulations.

(E) Cytotoxic T cells ($CD8^+IFN\gamma^+$), (F) CD8 effector T cells ($CD8^+CD44^+CD62L^-$), and (G) Regulatory cells ($T_R$, $CD4^+CD25^+Foxp3^+$) in tumor tissue examined by flow cytometry.

(H) Cumulative survival curves of tumor mice, (n = 7).

(I) H&E staining of the tumor tissues with different treatments, scale bar = 200 μm. Caspase-3 (red fluorescence) and $CD8^+$ T cells (green fluorescence) in tumor tissues, scale bar = 50 μm. Data are presented as mean ± S.D, ***$p < 0.001$, **$p < 0.01$, and *$p < 0.05$.

immune-fluorescent staining (Figure 5I). Enhanced fluorescent intensity of caspase-3 and $CD8^+$ in the T-D group showed a strong antitumor immune activity. These results collectively proved that the robust antitumor immune response was developed in tumor owning to long-term immune memory effects of T-D-treated cell vaccine, naturally, which also indicated that T-D is an excellent ICD inducer with the specific function of trigging vigorous oxidative stress in mitochondria.

## Therapeutic effect of T-D treated cell vaccine combined with anti-PDL1

To further evaluate the efficacy of the T-D-treated cell vaccine, we performed a study in which subcutaneous tumors in mice were treated with T-D-treated cell vaccine in combination with anti-PDL1. As shown in Figure 6A, tumor growth in mice treated with T-D-treated cell vaccine + anti-PDL1 was significantly impaired when compared with mice treated with T-D treated cell vaccine or anti-PDL1 alone. In Figure 6B, the volume of tumors in mice treated with T-D-treated cell vaccine + anti-PDL1 was almost significantly inhibited (615 $mm^3$), which was 3.1-, 2.6- and 1.9-fold lower than that of the Control group (1912 $mm^3$), anti-PDL1 group (1586 $mm^3$) and T-D-treated cell vaccine group (1149 $mm^3$), respectively. Furthermore, a comparable trend was observed in the analysis of tumor weight (Figure 6C). The tumor weight is

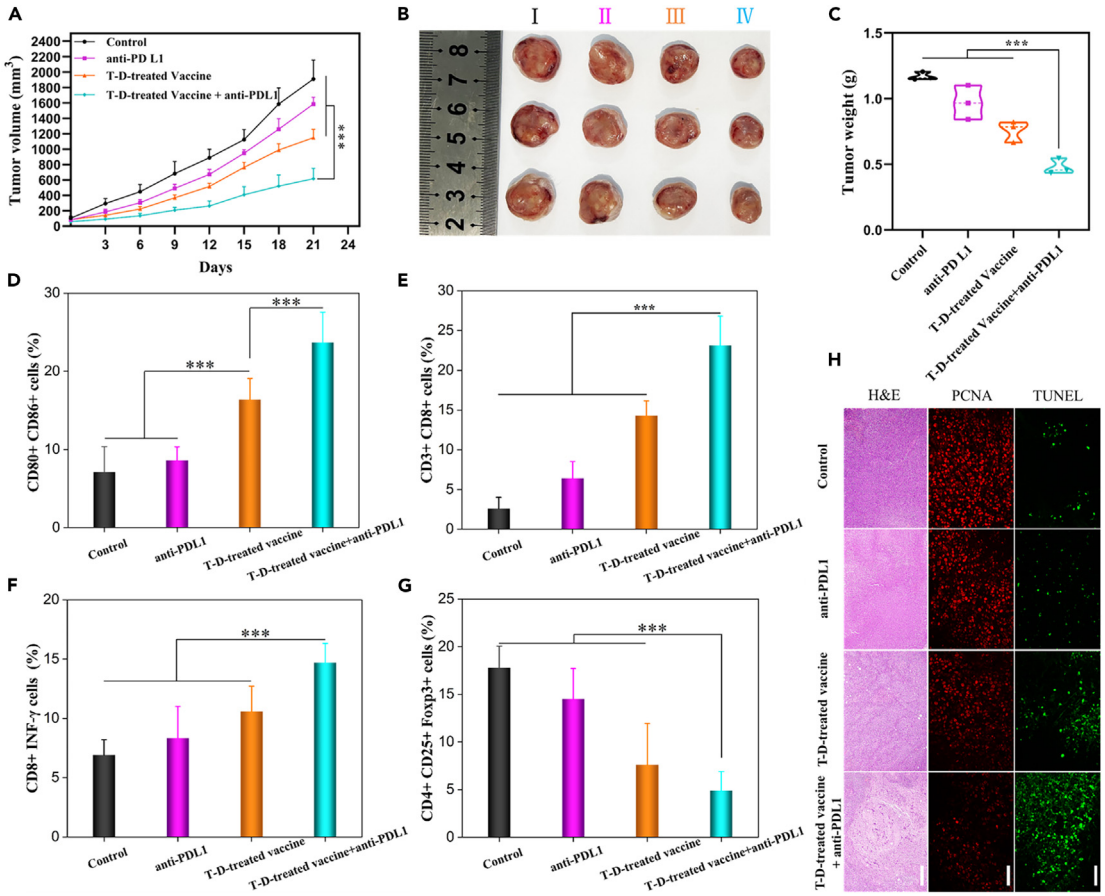


**Figure 6. Mice were treated with T-D-treated cell vaccine in combination with anti-PDL1**

(A) Average tumor growth curves of mice in different treatment groups, (n = 8).

(B) Tumor images after different treatments. I, Control; II, anti-PDL1; III, T-D-treated vaccine; IV, T-D-treated vaccine+anti-PDL1.

(C) Tumor weights of extracted tumors from different groups, (n = 3).

(D) Quantitative analysis of the proportion of mature DCs in inguinal lymph nodes of mice after different treatments.

(E) $CD3^+CD8^+$, (F) $CD8^+IFN\gamma^+$, and (G) $CD4^+CD25^+Foxp3^+$ T cells in tumor sections.

(H) H&E, scale bar = 200 μm, PCNA, and TUNEL-stained tumor slides, scale bar = 50 μm. Data are presented as mean ± S.D, ***$p < 0.001$, **$p < 0.01$, and *$p < 0.05$.

reduced from 1.17 g in the Control group to 0.97 g, 0.76 g, and 0.48 g after treatment with anti-PD-L1 antibody, T-D-treated cell vaccine, and T-D-treated cell vaccines + anti-PDL1, respectively.

These exciting results prompted us to further evaluate immune cells in the lymph nodes and tumors. As shown in Figure 6D and Figure S19, the percentage of mature DCs is 23.7% after treatment with T-D-treated cell vaccines + anti-PD-L1 antibody, compared with 7.1% in the Control group, 16.4% in the T-D-treated cell vaccine group, and 8.6% in the group treated with the anti-PDL1 alone, mirroring that T-D-treated vaccine could stimulate DCs maturation. Additionally, $CD3^+$ $CD8^+$ T cell infiltration into the tumor were analyzed (Figure 6E). The ratio of $CD8^+$ T-cells were distinctively upregulated. $CD8^+$ IFN-$\gamma^+$ T cell plays a vital role in killing tumor cells. Of all the groups, the combination group had the highest proportion of $CD8^+$ IFN-$\gamma^+$ T cells and the lowest proportion of $T_R$ cells ($CD4^+CD25^+Foxp3^+$) T cells, 14.7%, and 4.9%, respectively (Figures 6F and 6G). Meanwhile, the favorable therapeutic effect was also verified by PCNA and TUNEL staining of tumor sections, as shown in Figure 6H. Additionally, there was no significant change in body weight during treatment (Figure S20). The T-D-treated cell vaccine + anti-PDL1 antibody group exhibited a greater proportion of dead cells in tumor tissues and weaker PCNA signals. These results indicated apparent tumor cell apoptosis and severely impaired the proliferation of tumor cells. Therefore, T-D-treated cell vaccines could be a promising ICD-associated vaccine to activate the tumor immune response and boost the therapeutic effect of anti-PD-L1 antibody.

## Biosafety of vaccines

During the tumor treatment, the side effects of the vaccines on the mice were directly evaluated by recording the changes in body weight of each group, as shown in Figure S21, no significant change in the body weight of mice in each group was observed. Additionally, the biosafety

of the vaccines were assessed. The heart, liver, spleen, kidney, and lung tissues of each group of mice were collected for H&E staining, as shown in Figure S22, no observable damage to major organs was found by the histomorphological analysis. In addition, the levels of total white blood cells (WBC), total red blood cells (RBC), hemoglobin content (HGB), red blood cell volume (MCV), red blood cell hemoglobin concentration (MCHC), and platelets (PLT) in blood samples taken from the Control, X-ray, DHA and T-D groups of mice will be analyzed for blood routine (Figure S23). No detectable changes in blood biochemical indexes were observed for the tested dose, indicating that these vaccines have good biosafety *in vivo*.

## DISCUSSION

A mitochondria-targeting dihydroartemisinin derivative TPP-DHA (T-D) was synthesized. T-D accumulation in the mitochondria is a prerequisite for the generation of mitochondria-localized ROS, which contributed to the good realization of its ICD property. Compared to DHA, T-D was a ROS supergenerator that not merely augments ROS production in mitochondria but also induces a stronger release of immunogenic DAMPs. In more detail, the superior immunogenicity of T-D is attributed to the activation of the PERK signaling pathway. *In vivo*, T-D-treated cell vaccine can efficiently promote DCs maturation, tumor-specific cytotoxic T lymphocyte proliferation, as well as a large-scale release of proinflammatory cytokines such as IL-6, TNF-$\alpha$, and IFN-$\gamma$. Intriguingly, in vaccination assay, the rate of tumor inhibition and survival in mice confirmed that T-D-treated cell vaccine provokes the body to develop an immune response, form a long-term immune memory, and have excellent tumor prevention effects. Furthermore, in therapeutic vaccine trials, the combination of T-D-treated cell vaccine and anti-PDL1 exhibited favorable anti-tumor therapeutic effects, suggesting that T-D-treated cell vaccine activates the immune response, increases T cell infiltration at the tumor site as well as enhances the tumor killing effect with the assistance of anti-PDL1. Taken together, T-D is a mitochondrion ROS-mediated ICD inducer, which provides an approach for the application of artemisinin-based drugs in the ICD field, and we hope this study will be an inspiration for applying artemisinin analogs to chemo-immunotherapeutic agents.

### Limitations of the study

We synthesized a mitochondria-targeted dihydroartemisinin derivative, T-D, and found that it significantly induced immu-nogenic cell death, and demonstrated that T-D is a immunogenic death inducer by vaccine experiments. Whether better anticancer effects would be obtained if the treatment was administered by injection has not been explored, and we are in the process of doing this.

## STAR★METHODS

Detailed methods are provided in the online version of this paper and include the following:

- KEY RESOURCES TABLE
- RESOURCE AVAILABILITY
  - Lead contact
  - Materials availability
  - Data and code availability
- EXPERIMENTAL MODEL AND SUBJECT DETAILS
  - Animals and tumor models
  - Cell culture
- METHOD DETAILS
  - Synthesis and characterization of TPPBr-$(CH_2)_4$-COOH and TPP-DHA
  - Cytotoxicity *in vitro*
  - Apoptosis assay
  - Intramitochondrial ROS generation
  - Evaluation of mitochondrial depolarization
  - ICD effects *in vitro*
  - Analysis of apoptosis-related proteins
  - Preparation of tumor cell vaccine
  - Induction of dendritic cell maturation and detection of cytokine secretion *in vitro*
  - Vaccination
  - Immune cells analysis and suppression of tumor metastasis *in vivo*
  - Anticancer efficacy
  - Therapeutic vaccine research
  - Biosafety assessment *in vivo*
- QUANTIFICATION AND STATISTICAL ANALYSIS

## SUPPLEMENTAL INFORMATION

Supplemental information can be found online at https://doi.org/10.1016/j.isci.2023.108702.

## ACKNOWLEDGMENTS

This work was supported by the National Natural Science Foundation of China (52173137, 51873163).

## AUTHOR CONTRIBUTIONS

S.H. conceived and designed the study. H.Z., K.L., D.W., Z.Z., Z.X., and M.Q. contribute to conducting the investigation. H.Z., K.L., D.W., and Z.Z. contribute to analysis of data. H.Z. contribute to writing the article, H.Z. and S.H. revised the article.

## DECLARATION OF INTERESTS

The authors declare no competing interests.

Received: September 6, 2023
Revised: November 7, 2023
Accepted: December 6, 2023
Published: December 9, 2023

## REFERENCES

1. Huang, G., Liu, L., Pan, H., and Cai, L. (2023). Biomimetic Active Materials Guided Immunogenic Cell Death for Enhanced Cancer Immunotherapy. Small Methods *7*, e2201412.
2. Sen, S., Won, M., Levine, M.S., Noh, Y., Sedgwick, A.C., Kim, J.S., Sessler, J.L., and Arambula, J.F. (2022). Metal-based anticancer agents as immunogenic cell death inducers: the past, present, and future. Chem. Soc. Rev. *51*, 1212–1233.
3. Li, W., Yang, J., Luo, L., Jiang, M., Qin, B., Yin, H., Zhu, C., Yuan, X., Zhang, J., Luo, Z., et al. (2019). Targeting photodynamic and photothermal therapy to the endoplasmic reticulum enhances immunogenic cancer cell death. Nat. Commun. *10*, 3349.
4. Kroemer, G., Galassi, C., Zitvogel, L., and Galluzzi, L. (2022). Immunogenic cell stress and death. Nat. Immunol. *23*, 487–500.
5. Ding, D., and Jiang, X. (2023). Advances in Immunogenic Cell Death for Cancer Immunotherapy. Small Methods *7*, e2300354.
6. Zhou, J., Wang, G., Chen, Y., Wang, H., Hua, Y., and Cai, Z. (2019). Immunogenic cell death in cancer therapy: Present and emerging inducers. J. Cell Mol. Med. *23*, 4854–4865.
7. Xie, D., Wang, Q., and Wu, G. (2022). Research progress in inducing immunogenic cell death of tumor cells. Front. Immunol. *13*, 1017400.
8. Dudek, A.M., Garg, A.D., Krysko, D.V., De Ruysscher, D., and Agostinis, P. (2013). Inducers of immunogenic cancer cell death. Cytokine Growth Factor Rev. *24*, 319–333.
9. Wei, D., Chen, Y., Huang, Y., Li, P., Zhao, Y., Zhang, X., Wan, J., Yin, X., Liu, T., Yin, J., et al. (2021). NIR-light triggered dual-cascade targeting core-shell nanoparticles enhanced photodynamic therapy and immunotherapy. Nano Today *41*, 101288.
10. Wang, Y., Wang, W., Gu, R., Chen, J., Chen, Q., Lin, T., Wu, J., Hu, Y., and Yuan, A. (2023). In Situ Vaccination with Mitochondria-Targeting Immunogenic Death Inducer Elicits CD8(+) T Cell-Dependent Antitumor Immunity to Boost Tumor Immunotherapy. Adv. Sci. *10*, e2300286.
11. Wang, L., Guan, R., Xie, L., Liao, X., Xiong, K., Rees, T.W., Chen, Y., Ji, L., and Chao, H. (2021). An ER-Targeting Iridium(III) Complex That Induces Immunogenic Cell Death in Non-Small-Cell Lung Cancer. Angew. Chem., Int. Ed. Engl. *60*, 4657–4665.
12. Li, J., Gao, H., Liu, R., Chen, C., Zeng, S., Liu, Q., and Ding, D. (2020). Endoplasmic reticulum targeted AIE bioprobe as a highly efficient inducer of immunogenic cell death. Sci. China Chem. *63*, 1428–1434.
13. Zhang, M., Jin, X., Gao, M., Zhang, Y., and Tang, B.Z. (2022). A Self-Reporting Fluorescent Salicylaldehyde-Chlorambucil Conjugate as a Type-II ICD Inducer for Cancer Vaccines. Adv. Mater. *34*, e2205701.
14. Gao, Z., Jia, S., Ou, H., Hong, Y., Shan, K., Kong, X., Wang, Z., Feng, G., and Ding, D. (2022). An Activatable Near-Infrared Afterglow Theranostic Prodrug with Self-Sustainable Magnification Effect of Immunogenic Cell Death. Angew. Chem., Int. Ed. Engl. *61*, e202209793.
15. Yang, Q.Y., Ma, R., Gu, Y.Q., Xu, X.F., Chen, Z.F., and Liang, H. (2022). Arene-Ruthenium(II)/Osmium(II) Complexes Potentiate the Anticancer Efficacy of Metformin via Glucose Metabolism Reprogramming. Angew. Chem., Int. Ed. Engl. *61*, e202208570.
16. Xiong, X., Huang, K.-B., Wang, Y., Cao, B., Luo, Y., Chen, H., Yang, Y., Long, Y., Liu, M., Chan, A.S.C., et al. (2022). Target Profiling of an Iridium(III)-Based Immunogenic Cell Death Inducer Unveils the Engagement of Unfolded Protein Response Regulator BiP. J. Am. Chem. Soc. *144*, 10407–10416.
17. Wang, T., Gao, Z., Zhang, Y., Hong, Y., Tang, Y., Shan, K., Kong, X., Wang, Z., Shi, Y., and Ding, D. (2022). A supramolecular self-assembled nanomaterial for synergistic therapy of immunosuppressive tumor. J. Contr. Release *351*, 272–283.
18. Kraus, F., Roy, K., Pucadyil, T.J., and Ryan, M.T. (2021). Function and regulation of the divisome for mitochondrial fission. Nature *590*, 57–66.
19. Arruda, A.P., Pers, B.M., Parlakgül, G., Güney, E., Inouye, K., and Hotamisligil, G.S. (2014). Chronic enrichment of hepatic endoplasmic reticulum-mitochondria contact leads to mitochondrial dysfunction in obesity. Nat. Med. *20*, 1427–1435.
20. Marchi, S., Patergnani, S., Missiroli, S., Morciano, G., Rimessi, A., Wieckowski, M.R., Giorgi, C., and Pinton, P. (2018). Mitochondrial and endoplasmic reticulum calcium homeostasis and cell death. Cell Calcium *69*, 62–72.
21. Burgos-Morón, E., Abad-Jiménez, Z., Marañón, A.M.d., Iannantuoni, F., Escribano-López, I., López-Domènech, S., Salom, C., Jover, A., Mora, V., Roldan, I., et al. (2019). Relationship Between Oxidative Stress, ER Stress, and Inflammation in Type 2 Diabetes: The Battle Continues. J. Clin. Med. *8*, 1385.
22. Zheng, P., Ding, B., Zhu, G., Li, C., and Lin, J. (2022). Biodegradable Ca(2+) Nanomodulators Activate Pyroptosis through Mitochondrial Ca(2+) Overload for Cancer Immunotherapy. Angew. Chem., Int. Ed. Engl. *61*, e202204904.
23. Zheng, P., Ding, B., Jiang, Z., Xu, W., Li, G., Ding, J., and Chen, X. (2021). Ultrasound-Augmented Mitochondrial Calcium Ion Overload by Calcium Nanomodulator to Induce Immunogenic Cell Death. Nano Lett. *21*, 2088–2093.
24. Liao, L.-S., Chen, Y., Hou, C., Liu, Y.-H., Su, G.-F., Liang, H., and Chen, Z.-F. (2023). Potent Zinc(II)-Based Immunogenic Cell Death Inducer Triggered by ROS-Mediated ERS and Mitochondrial $Ca^{2+}$ Overload. J. Med. Chem. *66*, 10497–10509.
25. Chen, C., Ni, X., Jia, S., Liang, Y., Wu, X., Kong, D., and Ding, D. (2019). Massively Evoking Immunogenic Cell Death by Focused Mitochondrial Oxidative Stress using an AIE Luminogen with a Twisted Molecular Structure. Adv. Mater. *31*, e1904914.
26. Jia, S., Gao, Z., Wu, Z., Gao, H., Wang, H., Ou, H., and Ding, D. (2022). Sonosensitized Aggregation-Induced Emission Dots with Capacities of Immunogenic Cell Death Induction and Multivalent Blocking of Programmed Cell Death-Ligand 1 for Amplified Antitumor Immunotherapy. CCS Chem. *4*, 501–514.
27. Li, K.-H., Zhao, H.-Y., Wang, D.-D., Qi, M.-H., Xu, Z.-J., Li, J.-M., Zhang, Z.-L., and Huang, S.-W. (2023). Mitochondria-targeted nano-AIEgens as a powerful inducer for evoking immunogenic cell death. Chin. Chem. Lett. 108882.
28. Tu, Y. (2016). Artemisinin-A Gift from Traditional Chinese Medicine to the World (Nobel Lecture). Angew. Chem., Int. Ed. Engl. *55*, 10210–10226.
29. Wan, X., Zhong, H., Pan, W., Li, Y., Chen, Y., Li, N., and Tang, B. (2019). Programmed Release of Dihydroartemisinin for Synergistic Cancer Therapy Using a CaCO3 Mineralized

Metal-Organic Framework. Angew. Chem., Int. Ed. Engl. *58*, 14134–14139.

30. Zhang, C.J., Wang, J., Zhang, J., Lee, Y.M., Feng, G., Lim, T.K., Shen, H.M., Lin, Q., and Liu, B. (2016). Mechanism-Guided Design and Synthesis of a Mitochondria-Targeting Artemisinin Analogue with Enhanced Anticancer Activity. Angew. Chem., Int. Ed. Engl. *55*, 13770–13774.
31. Xu, C., Xiao, L., Lin, P., Yang, X., Zou, X., Mu, L., and Yang, X. (2022). Synthesis and Antitumor Activities of Novel Mitochondria-Targeted Dihydroartemisinin Ether Derivatives. ACS Omega *7*, 38832–38846.
32. Xu, C., Xiao, L., Zhang, X., Zhuang, T., Mu, L., and Yang, X. (2021). Synthesis and biological activities of novel mitochondria-targeted artemisinin ester derivatives. Bioorg. Med. Chem. Lett. *39*, 127912.
33. Duan, X., Chan, C., Han, W., Guo, N., Weichselbaum, R.R., and Lin, W. (2019). Immunostimulatory nanomedicines synergize with checkpoint blockade immunotherapy to eradicate colorectal tumors. Nat. Commun. *10*, 1899.
34. Yu, H., Li, J.M., Deng, K., Zhou, W., Wang, C.X., Wang, Q., Li, K.H., Zhao, H.Y., and Huang, S.W. (2019). Tumor acidity activated triphenylphosphonium-based mitochondrial targeting nanocarriers for overcoming drug resistance of cancer therapy. Theranostics *9*, 7033–7050.
35. Zorov, D.B., Juhaszova, M., and Sollott, S.J. (2014). Mitochondrial reactive oxygen species (ROS) and ROS-induced ROS release. Physiol. Rev. *94*, 909–950.
36. Wong, D.Y.Q., Ong, W.W.F., and Ang, W.H. (2015). Induction of immunogenic cell death by chemotherapeutic platinum complexes. Angew. Chem., Int. Ed. Engl. *54*, 6483–6487.
37. Ahmed, A., and Tait, S.W.G. (2020). Targeting immunogenic cell death in cancer. Mol. Oncol. *14*, 2994–3006.
38. Chen, R., Kang, R., and Tang, D. (2022). The mechanism of HMGB1 secretion and release. Exp. Mol. Med. *54*, 91–102.
39. Wang, Y., Qi, H., Liu, Y., Duan, C., Liu, X., Xia, T., Chen, D., Piao, H.L., and Liu, H.X. (2021). The double-edged roles of ROS in cancer prevention and therapy. Theranostics *11*, 4839–4857.
40. Nakamura, H., and Takada, K. (2021). Reactive oxygen species in cancer: Current findings and future directions. Cancer Sci. *112*, 3945–3952.
41. Chen, X., and Cubillos-Ruiz, J.R. (2021). Endoplasmic reticulum stress signals in the tumour and its microenvironment. Nat. Rev. Cancer *21*, 71–88.
42. Ong, G., and Logue, S.E. (2023). Unfolding the Interactions between Endoplasmic Reticulum Stress and Oxidative Stress. Antioxidants *12*.
43. Feng, X., Lin, T., Chen, D., Li, Z., Yang, Q., Tian, H., Xiao, Y., Lin, M., Liang, M., Guo, W., et al. (2023). Mitochondria-associated ER stress evokes immunogenic cell death through the ROS-PERK-eIF2alpha pathway under PTT/CDT combined therapy. Acta Biomater. *160*, 211–224.
44. Xu, Y.D., Cheng, M., Shang, P.P., and Yang, Y.Q. (2022). Role of IL-6 in dendritic cell functions. J. Leukoc. Biol. *111*, 695–709.
45. Speiser, D.E., Chijioke, O., Schaeuble, K., and Münz, C. (2023). CD4(+) T cells in cancer. Nat. Can. (Ott.) *4*, 317–329.
46. Philip, M., and Schietinger, A. (2022). CD8(+) T cell differentiation and dysfunction in cancer. Nat. Rev. Immunol. *22*, 209–223.
47. Chang, J.T., Wherry, E.J., and Goldrath, A.W. (2014). Molecular regulation of effector and memory T cell differentiation. Nat. Immunol. *15*, 1104–1115.
48. Kartikasari, A.E.R., Huertas, C.S., Mitchell, A., and Plebanski, M. (2021). Tumor-Induced Inflammatory Cytokines and the Emerging Diagnostic Devices for Cancer Detection and Prognosis. Front. Oncol. *11*, 692142.
49. Vazquez, M.I., Catalan-Dibene, J., and Zlotnik, A. (2015). B cells responses and cytokine production are regulated by their immune microenvironment. Cytokine *74*, 318–326.
50. Jin, M.Z., and Wang, X.P. (2021). Immunogenic Cell Death-Based Cancer Vaccines. Front. Immunol. *12*, 697964.

## STAR★METHODS

### KEY RESOURCES TABLE

| REAGENT or RESOURCE | SOURCE | IDENTIFIER |
|---|---|---|
| Antibodies | | |
| Rabbit anti-mouse calreticulin | StressMarq bioscience | Cat# SPC-122B; RRID: 2069601 |
| Rabbit anti-mouse HMGB-1 | BioLegend | Cat# 651403; RRID: AB_2562220 |
| Rabbit anti-mouse CD11c | BioLegend | Cat# 117310; RRID: AB_313779 |
| Rabbit anti-mouse CD80 | BioLegend | Cat# 104705; RRID: AB_313126 |
| Rabbit anti-mouse CD86 | BioLegend | Cat# 159203; RRID: AB_2832567 |
| Rabbit anti-mouse CD45 | BD Biosciences | Cat# 557659; RRID: AB_396774 |
| Rabbit anti-mouse CD3 | BD Biosciences | Cat# 561798; RRID: AB_10898341 |
| Rabbit anti-mouse CD4 | BD Biosciences | Cat# 561832; RRID: AB_10893224 |
| Rabbit anti-mouse CD8 | BD Biosciences | Cat# 553035; RRID: AB_398527 |
| Rabbit anti-mouse CD44 | BD Biosciences | Cat# 563114; RRID: AB_2738011 |
| Rabbit anti-mouse CD62L | BD Biosciences | Cat# 564108; RRID: AB_2738597 |
| Rabbit anti-mouse INFγ | BD Biosciences | Cat# 557649: RRID: AB_396766 |
| Rabbit anti-mouse FOXP3 | BD Biosciences | Cat# 562996: RRID: AB_2737940 |
| Anti-PDL1 | BioLegend | Cat# 123418: RRID: AB_1953275 |
| Chemicals, peptides, and recombinant proteins | | |
| Triphenylphosphine | Innochem | A37091 |
| 5-bromovaleric acid | Alfa aesar | A11765 |
| Dihydroartemisinin | TCI | D3793 |
| Dicyclohexylcarbodiimide | Aladdin | D106074 |
| 4-dimethylaminopyridine | Aladdin | D109207 |
| Acetonitrile | Sinopharm | 80000608 |
| Dichloromethane | Sinopharm | 80047318 |
| Critical commercial assays | | |
| AnnexinV-FITC/PI assay Kits | Genview® | GK3603-20T |
| Calcein-AM/PI staining analysis Kit | Solarbio® Life Science | CA1630 |
| ATP Elisa assay Kit | MSKBIO | N/A |
| Reactive oxygen Species Assay Kit | Genview® | GK3611 |
| Mito-Tracker Red CMXRos Kit | Beyotime | C1049 |
| Deposited data | | |
| Raw data | This paper | https://doi.org/10.17632/bcyc32c6zx.1 |
| Experimental models: Cell lines | | |
| 4T1 | Haixing Biosciences | TCM-C705 |
| Experimental models: Organisms/strains | | |
| Female mice (BLAB/c) | Liaoningchangsheng biotechnology | 210726230101224227 |
| Software and algorithms | | |
| FlowJo v10.5.3 | BD Biosciences | https://www.flowjo.com/ |
| GraphPad Prism 8.0 | GraphPad | https://www.graphpad.com |
| ImageJ | ImageJ | https://imagej.net/ij/ |
| Origin2021 | Origin | https://www.originlab.com/ |

(*Continued on next page*)

*Continued*

| REAGENT or RESOURCE | SOURCE | IDENTIFIER |
|---|---|---|
| Other | | |
| Nuclear magnetic resonance spectrometer | Bruker | AV II-400 MHz |
| Microplate reader | Molecular Devices | Spectra MaxiD3 |
| Fluorescent inverted microscope | Leica | DMi8 |
| Flow cytometer | Beckman coulter | Cytoflex $V_2$-$B_4$-$R_2$ |
| Laser scanning confocal microscope | Andor | Andor Revolution XD |

## RESOURCE AVAILABILITY

### Lead contact

Further information and requests for resources should be directed to and will be fulfilled by the lead contact, Shiwen Huang (swhuang@whu.edu.cn).

### Materials availability

New unique reagents were not produced in this work.

### Data and code availability

- Data reported in this paper will be shared by the lead contact upon request.
- This paper does not report original code.
- Any additional information required to reanalyze the data reported in this work paper is available from the lead contact upon request

## EXPERIMENTAL MODEL AND SUBJECT DETAILS

### Animals and tumor models

Female mice (BLAB/c, 5 weeks old, 16 to 18 g) were provided by Liaoning changsheng biotechnology Co., Ltd (Liaoning, China) and held under specific pathogen-free conditions. To build a tumor model, 4T1 cells ($1\times10^6$ cells in 100 μL of PBS) were injected into the right flank region of mice. All animal experiments involved in this paper were conducted following the Laboratory Animal Guidelines established by the Wuhan University Animal Center Experiment/A3-Lab, and the study protocols were approved by the Experimental Animal Welfare and Ethics of the Zhongnan Hospital of Wuhan University (ZN2021232).

### Cell culture

Breast cancer 4T1 cells were purchased from the Haixing Biosciences Co., Ltd (Jiangsu, China) and incubated in RPMI 1640 medium which is added with 10% fetal bovine serum (FBS), 1% penicillin, and 1% streptomycin. Cells were placed in an incubator with a humidified atmosphere containing 5% $CO_2$ at 37°C.

## METHOD DETAILS

### Synthesis and characterization of TPPBr-$(CH_2)_4$-COOH and TPP-DHA

Triphenylphosphine (1.6 g, 6.1 mmol) and 5-bromovaleric acid (1.0 g, 5.5 mmol) were added to anhydrous acetonitrile (30 mL), and the resulting mixture was refluxed at 85°C for 24 h. After the reaction was finished, a row product (TPPBr-$(CH_2)_4$-COOH) was obtained after removing acetonitrile by using a vacuum rotary evaporator. The resulting white viscous solid was dissolved in dichloromethane (10 ml), then the solution was added to cool diethyl ether (200 ml) slowly for stirring and recrystallizing, the white precipitate was collected by pumping filtration. Repeat this process 2 or 3 times. Afterward, the final product was obtained through vacuum drying as a white solid with a 66.7% yield.

TPPBr-$(CH_2)_4$-COOH (2.84 g, 4 mmol) and 4-dimethylaminopyridine (244.3 mg, 2 mmol) were dissolved in distilled dichloromethane under ice bath (30 ml), a solution of dicyclohexylcarbodiimide (824.7 mg, 4 mmol) in distilled dichloromethane was slowly dripped into the solutions described above and kept stirring. To that mixture was added dihydroartemisinin (995.2 mg, 3.5 mmol), and then the reaction was carried out for 24 h under nitrogen protection. After filtering the reaction solution to remove the white suspensions of DCU, a clear solution was obtained. Then a white product (TPP-DHA, T-D) was gained after the filtrate removed dichloromethane by using a vacuum rotary evaporator and washed with distilled water repeatedly, resulting in a yield of 62% after lyophilized. The structure of TPPBr-$(CH_2)_4$-COOH and TPP-DHA were analyzed by $^1$H NMR spectrophotometry.

### Cytotoxicity *in vitro*

4T1 cells were seeded in a 96-well plate at a density of $3\times10^3$ cells per well and allowed to adhere for 24 h. Cells were then treated respectively with 100 μL of medium containing equimolar concentration of free DHA and free T-D. After incubation for 48 h, 20 μL thiazolyl blue solution was added to every well and incubated with cells for 4 h. Then the culture medium in each well was removed completely and dimethyl sulfoxide (150 μL) was used to dissolve the formazan crystals generated by living cells. Cells incubated with fresh RPMI-1640 medium were used as a control. The absorbance at 570 nm was measured by a microplate reader. Cell viability was calculated following the standard method of MTT.

### Apoptosis assay

4T1 cells were planted in 6-well plates at a density of $1\times10^5$ cells in each well and allowed to adhere for 24 h. Then the original medium in per well was removed completely and replaced by 2 mL of medium containing free DHA (2.5 μM) or free T-D (2.5 μM). After incubation with drugs for 24 h, the medium was removed and each well was rinsed thoroughly with PBS buffer. Afterward, the cells were stained by Calcein-AM/PI, followed by analysis using an inverted fluorescence microscope. Moreover, Annexin-FITC/PI double staining test also was chosen to assess apoptosis. Briefly, Cells were seeded and treated as above, then harvested, and rinsed once with PBS buffer. Subsequently, the cells were stained with Annexin V-FITC/PI according to the manufacturer's instructions and then analyzed with flow cytometry.

### Intramitochondrial ROS generation

4T1 cells were cultured in glass-bottom dishes ($1\times10^5$ per dish) for 24 h. The previous medium was replaced with a fresh medium containing DCFH-DA (10 μM). After 30 min incubation, to remove the extracellular DCFH-DA, the cells were rinsed thoroughly with serum-free medium and treated with culture medium containing free DHA (2.5 μM) or free T-D (2.5 μM) for 6 h, 12 h, 18 h, and 24 h respectively. After treatment, cells were gently washed with PBS three times and stained with 100 nM Mito-trackerRed CMXRos for 15 min at room temperature in the dark. Subsequently, PBS washed away the unloaded Mito-tracker Red probes, and then cells were observed under CLSM using 488 nm and 561 nm lasers for visualizing ROS generation and mitochondria respectively. Meanwhile, mitochondrial ROS production was quantitatively analyzed by flow cytometry. In brief, cells were seeded in 6-well plates and treated as above, then harvested and analyzed with flow cytometry, cells with no treatment were used as controls.

### Evaluation of mitochondrial depolarization

4T1 cells were seeded into glass-bottom dishes ($1\times10^5$ per dish), cultured overnight, and then treated with 2 mL of fresh medium containing free DHA (2.5 μM) or free T-D (2.5 μM) for 12 h, and 24 h, respectively. Afterward, the cell supernatant was discarded and the cells were stained with a medium containing 10 μg/mL JC-1 dye for 15 min at 37°C in the dark. After that, the medium was removed, and the cells were rinsed thoroughly with PBS to remove the unloaded JC-1 probes. Finally, cells were observed under CLSM using 488 nm and 561 nm lasers for visualizing the green fluorescence of J-monomer and the red fluorescence of J-aggregates, respectively. Simultaneously, mitochondrial depolarization was quantitatively analyzed. Cells were seeded in 6-well plates and treated as above, then harvested and analyzed with flow cytometry. Cells with no treatment were used as controls.

### ICD effects *in vitro*

4T1 cells were planted in 6-well plates at a density of $1\times10^5$ cells each well and allowed to adhere for 24 h, and then treated with 2 mL of fresh medium containing free T-D (0.5 μM, 1 μM, 2 μM, 2.5 μM, 3 μM) for 12 h, and 24 h, respectively. Following the manufacturer's protocol, cells were harvested and incubated with FITC-labeled anti-mouse calreticulin antibody (dilution 1:1000) for 30 min at room temperature in the dark. After that, cells were rinsed with PBS three times and re-collected by using a centrifuge at 2000 rpm for 5 min, then the calreticulin of the cell surface was utilized to analyze quantitatively by flow cytometry. Accordingly, for CLSM imaging of the CRT expression, cells were seeded in glass-bottom dishes and treated with different concentrations of T-D or DHA for 24 h as above. After applying FITC labeled anti-mouse calreticulin antibody and Hochest33342 stain, cells were finally observed by CLSM using 405 nm and 488 nm lasers for visualizing the nucleus and calreticulin respectively.

After seeded and cultured for 24 h in glass-bottom dishes ($1\times10^5$ cells per dish) to reach a confluence of 80%, cells were treated with 2 mL of fresh medium containing free DHA (2.5 μM) or free T-D (2.5 μM) for 12 h, the no treated cells were used as a control. After the end of co-cultivation, the cell supernatant was collected for detection of extracellular released ATP by ELISA according to the manufacturer's protocols, three parallel dishes were set for each group. For CLSM imaging of HMGB1, APC labeled anti-mouse HMGB1 antibody (dilution 1:500) was added to each dish and incubated for 30 min at room temperature in the dark. Then, the cells were washed with PBS and fixed with 4% paraformaldehyde for 10 min. After fixation, the cells were washed with PBS again and stained with Hochest33342 for 8 min at room temperature in the dark, followed by CLSM using 405 nm and 561 nm lasers for visualizing the nucleus and HMGB1 respectively.

### Analysis of apoptosis-related proteins

4T1 cells were planted in 6-well plates at a density of $1\times10^5$ cells each well for 24 h, and then treated with culture medium containing free DHA (2.5 μM) or free T-D (2.5 μM) for 24 h, the control group cells did not any treatment. Afterward, the cells were harvested and lysed with lysis buffer at 4°C for 10 min, cell lysate was centrifuged at 12,000 rpm for 5 min and protein content in supernatant was measured using an

enhanced BCA Protein Assay Kit. The lysates with equal amounts of protein were separated by SDS-PAGE and transferred to PVDF membranes. Membranes were blocked with 5% skim milk for 2 h and then incubated with cleaved caspase-3, p-PERK, PERK and β-Actin antibody at 4°C overnight, followed by horseradish peroxidase-conjugated secondary antibody treatment for 1 h at room temperature. Finally, the proteins were detected, and the chemiluminescence signals were visualized.

### Preparation of tumor cell vaccine

According to the results of the calreticulin induction assay *in vitro*, T-D, a mitochondria-targeting drug, could induce the highest calreticulin expression in 4T1 cells after treatment for 24 h at a concentration of 2.5 μM, hence different 4T1 cell vaccines were obtained after treatment with T-D or non-mitochondria-targeting drug DHA. Briefly, 4T1 cells ($1 \times 10^5$ cells) were seeded into 6-well plates and incubated overnight at 37°C, and then treated with T-D (2.5 μM) and DHA (2.5 μM) for 24 h respectively. Afterward, cells treated with T-D, DHA, and no treatments were collected and all irradiated with X-ray (single-fraction irradiation of 60 Gy) to ensure that the cells were safe as the cell vaccines named "T-D-treated", "DHA-treated" and "X-ray-treated", respectively.

### Induction of dendritic cell maturation and detection of cytokine secretion *in vitro*

Bone marrow dendritic cells were obtained from the femur and tibia of BALB/c mice. After lysis of erythrocytes, cells were collected by centrifugation at 1200 rpm for 5 min and cultured in RPMI 1640 containing 10% FBS. The plates were gently shaken every two days, and a 3/4 volume of medium was replaced and supplemented with cytokines IL-4 (10 ng/mL) and GM-CSF (20 ng/mL) to induce bone marrow cells differentiation into bone marrow dendritic cells (BMDCs). After one week, the suspension cells and the adherent cells were harvested, then cells were collected by centrifugation at 1200 rpm for 5 min, re-suspended, and seeded in six-well plates at a density of $1 \times 10^5$ cells/well, while $1 \times 10^5$ 4T1 vaccine cells from T-D, DHA, and X-ray groups were added to each well, respectively, and PBS was used as a control treatment for 24 h. Then cells were collected, rinsed with PBS, followed by staining with anti-CD86-PE and anti-CD80-FITC antibodies for 30 min at 4°C, and detected by flow cytometry. To detect cytokines secreted by dendritic cells after antigen uptake, such as interleukin 6 (IL-6) and tumor necrosis factor (TNF α). Simultaneously, cell culture supernatants from each of the above groups were collected, diluted to the appropriate ratio and tested according to the manufacturer's instructions, three independent samples were set for each group.

### Vaccination

The BALB/c mice aged 4–5 weeks were randomly divided into four groups, which were named "Control", "X-ray", "DHA", and "T-D", respectively. The corresponding 4T1 cancer vaccines were subcutaneously inoculated on the left flanks of mice in "X-ray", "DHA" and "T-D" groups, respectively. PBS was injected as the control. Each dose of vaccine for mice: $2 \times 10^6$ cells/mouse. The mice were vaccinated once a week two times in total and prepared for subsequent experiments.

### Immune cells analysis and suppression of tumor metastasis *in vivo*

One week after the second vaccination of mice in X-ray, DHA, and T-D groups. Subsequently, mice were randomly removed from Control, X-ray, DHA, and T-D group, and their blood was collected by cardiac puncture. Then mice were sacrificed, and their inguinal lymph nodes and spleens were collected. Mature DCs in lymph nodes and T cells in spleen were analyzed with flow cytometry. Briefly, lymph nodes were ground with the rubber end of a syringe and rinsed with PBS, cells were filtered through nylon mesh filters to harvest the single-cell suspension. Subsequently, cells were collected by centrifugation at 1200 rpm for 5 min and stained with anti-CD11c-APC, anti-CD86-PE, and anti-CD80-FITC antibodies for 30 min at 4°C, then washed twice with PBS, and analyzed by flow cytometry.

Similarly, the single-cell suspension from spleen was harvested according to the above method. After lysis of erythrocytes, cells were collected by centrifugation at 1200 rpm for 5 min and cultured in RPMI 1640 complete medium containing GolgiPlug stimulation blocker for 4 h in a $CO_2$ incubator, followed by incubation with anti-CD16/32 antibody for 10 min at 4°C. Then cells were collected by centrifugation and resuspended in a medium containing Fixable Viability Stain 700 for 5 min at 4°C. After that, cells were collected and rinsed with PBS, stained with stain buffer containing anti-CD45-APC-CY7 antibody, anti-CD3-FITC antibody, anti-CD4-PE antibody, anti-CD8-APC antibody, anti-CD44-BV510 antibody, and CD62L-BV650 antibody. Subsequently, cells were collected and rinsed with PBS again, treated with Fix/Perm buffer containing anti-IFNγ-PE-CY7 antibody for 40 min in the dark, and washed with Perm/Wash buffer. Finally, cells were collected and analyzed by flow cytometry.

Mice from Control, X-ray, DHA, and T-D group were injected with $5 \times 10^5$ live 4T1 cells through the tail vein. Two weeks after injection, mice were sacrificed, and their lungs were collected and analyzed by hematoxylin-eosin (H&E) staining for visualizing the metastatic foci. Simultaneously, the levels of immune-related cytokines in blood were evaluated, for instance, IL-6, TNF-α, and IFN-γ. Plasma was diluted to the appropriate ratio and determined by ELISA, three independent samples were set for each group.

### Anticancer efficacy

The experiment of vaccination, the gold standard, was used to further identify T-D as an ICD inducer. One week after the second vaccination of mice in X-ray, DHA, and T-D groups, $1 \times 10^6$ live 4T1 cells were subcutaneously injected into the right flank region of the remaining mice from Control, X-ray, DHA, and T-D groups. Tumor volume (V) and body weight were recorded every few days, and tumor volume was calculated as follows: $(\text{width}^2 \times \text{length})/2$. When the mean tumor volume of the Control group reached 2000 $mm^3$, three mice in each group were

randomly selected and sacrificed, tumors and inguinal lymph nodes were removed, and heart, liver, spleen, kidney, and lung tissues were collected for histological and immunohistochemical analyses, and DCs in lymph nodes and immune cells in tumor tissues were analyzed, as well as survival curves for the remaining mice in each group, experimental procedures refer to the above methods. Tumor inhibitory rate (TIR) was calculated as follows: TIR (%) = [1- ($V_{tf}$ - $V_{ti}$)/($V_{pf}$ - $V_{pi}$)] × 100, where $V_{tf}$ and $V_{ti}$ separately represent the final and initial tumor volume of the treated group, while $V_{pf}$ and $V_{pi}$ separately represent the final and initial tumor volume of the Control group. The mice with tumor volume reached 2000 $mm^3$ were considered dead and sacrificed.

### Therapeutic vaccine research

$1\times10^6$ live 4T1 cells were subcutaneously injected into the left flank region of mice. When the average tumor volume of the mice reached 80 $mm^3$, 8 mice in each group were randomly divided into 4 groups, which were named Control group, Anti-PDL1 group, T-D-treated vaccine group and T-D-treated vaccine + anti-PDL1 group. The mice were inoculated with T-D-treated cell vaccine ($2\times10^6$ cells/mouse) in the right flanks and intraperitoneally injected with anti-PDL1(1 mg/kg) the day after vaccination, a total of two times. Tumor volume (V) and body weight were recorded every three days, and tumor volume was calculated as follows: ($width^2$ × length)/2. When the mean tumor volume of the Control group reached 1900 $mm^3$, three mice in each group were randomly selected and sacrificed, tumors and inguinal lymph nodes were removed, DCs in lymph nodes and immune cells in tumor tissues were analyzed. Experimental procedures refer to the above methods. Tumor inhibitory rate (TIR) was calculated as follows: TIR (%) = [1- ($V_{tf}$ - $V_{ti}$)/($V_{pf}$ - $V_{pi}$)] × 100, where $V_{tf}$ and $V_{ti}$ separately represent the final and initial tumor volume of the treated group, while $V_{pf}$ and $V_{pi}$ separately represent the final and initial tumor volume of the Control group.

### Biosafety assessment *in vivo*

Healthy mice (non-tumor-bearing mice) inoculated with "X-ray-treated", "DHA-treated", and "T-D-treated" cell vaccines, respectively. Non-treated mice were used as a control. The mice were vaccinated once a week two times in total, then their blood samples were analyzed by an automated hematology analyzer for white blood cells (WBC), red blood cells (RBC), hemoglobin content (HGB), red blood cell volume (MCV), red blood cell hemoglobin concentration (MCHC) and platelets (PLT). Heart, liver, spleen, kidney, and lung tissues from each group of mice were performed separately to analyze the toxicity of vaccines on major organs.

## QUANTIFICATION AND STATISTICAL ANALYSIS

All statistical comparisons were performed by unpaired Student's *t* test or one-way ANOVA with Tukey's multiple comparisons test, statistical significance is displayed as: *$p < 0.05$; **$p < 0.01$; ***$p < 0.001$. All data were expressed as mean ± standard deviation (SD).